Supplementary Materials for

Spatially selective depletion of tumor-associated regulatory T cells with near-infrared photoimmunotherapy

This PDF file includes:

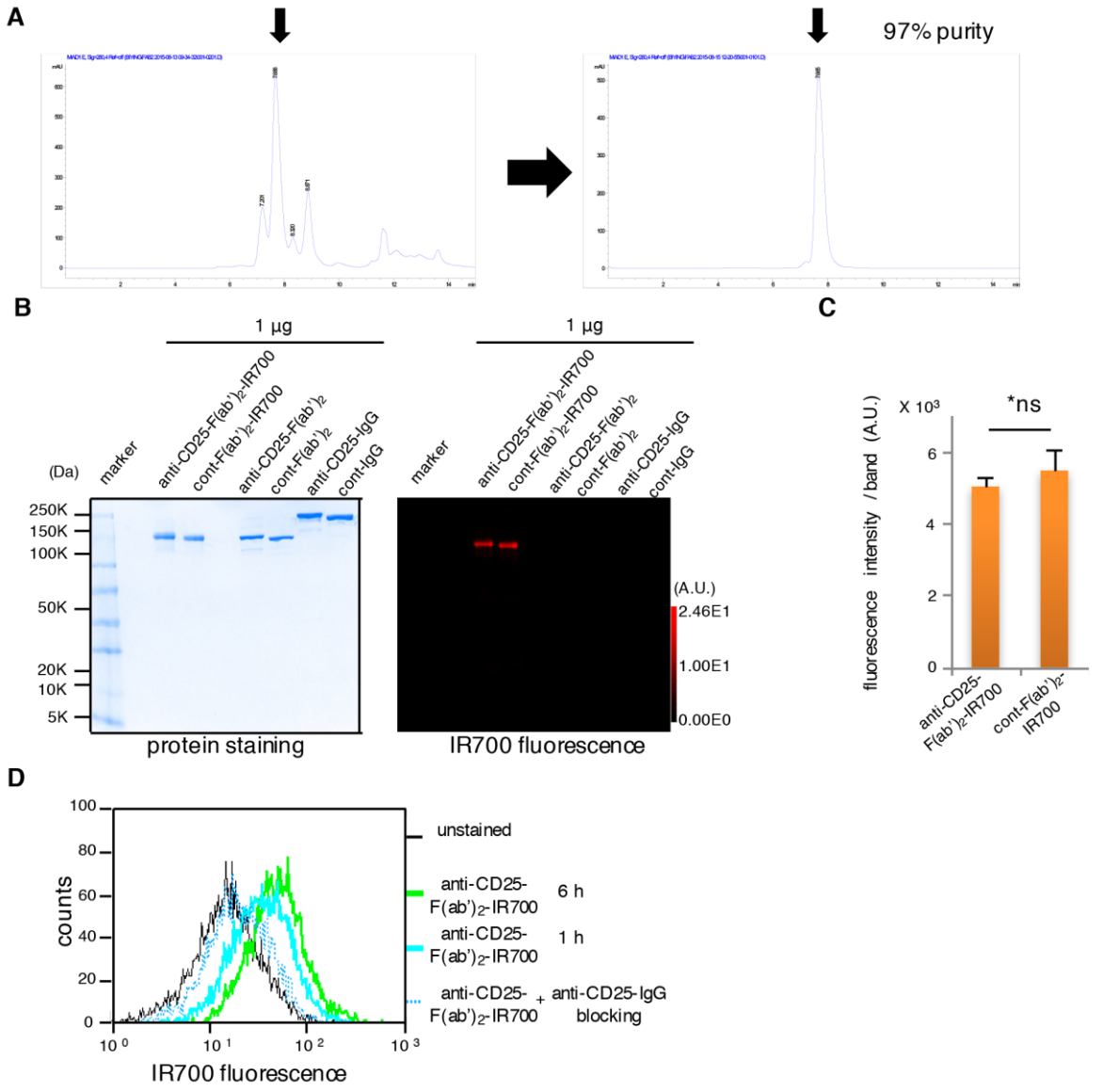

Supplementary Figure 1.

Anti-CD25-F(ab′)$_2$ and control-F(ab′)$_2$ are generated, characterized, and conjugated with IR700 dye.

(A) Anti-CD25-F(ab′)$_2$ was purified by HPLC after digestion of the intact antibody by ficin method. Left panel shows the HPLC profile of the digested antibody, and right panel shows

that of the anti-CD25-F(ab′)$_2$ with 97% purity. (B) SDS-PAGE analysis of anti-CD25-F(ab′)$_2$ and control-F(ab′)$_2$ digested from control IgG and their IR700 conjugates. Both anti-CD25-F(ab′)$_2$-IR700 and control-F(ab′)$_2$-IR700 bands showed similar IR700-fluorescence, which was confirmed by (C) quantitation of fluorescence intensity (n = 3; * ns, Mann-Whitney test). (D) The binding of the anti-CD25-F(ab′)$_2$-IR700 to CD25-expressing HT-2 A5E cells (T lymphocytes) was specific, and the addition of excess anti-CD25-IgG blocked its binding.

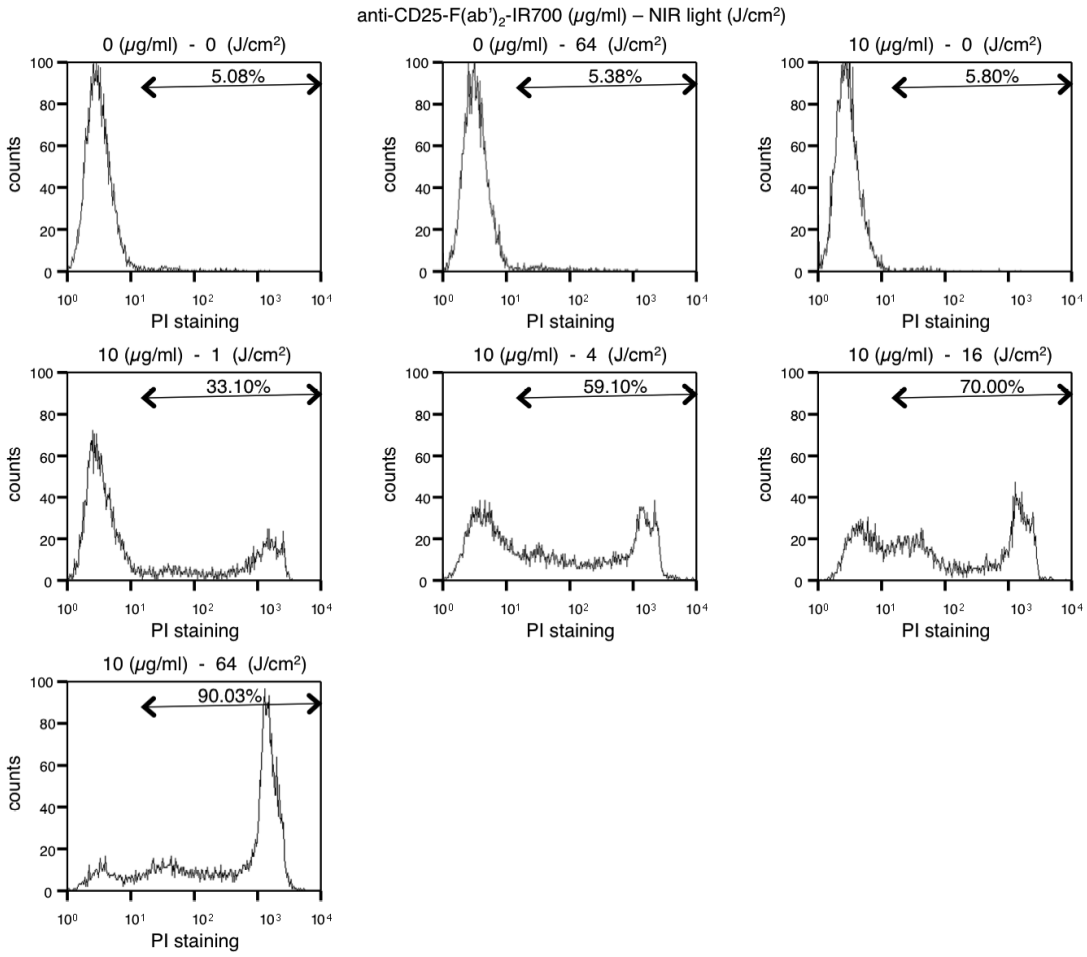

Supplementary Figure 2.

NIR-PIT with anti-CD25-F(ab′)$_2$–IR700 induces necrosis of CD25-expressing cells in a NIR light dose–dependent manner.

In vitro anti-CD25-F(ab′)$_2$–IR700 NIR-PIT against CD25-expressing HT-2 A5E cells induced necrotic death of these cells in a NIR light dose-dependent manner, as indicated by PI staining analyzed by flow cytometry.

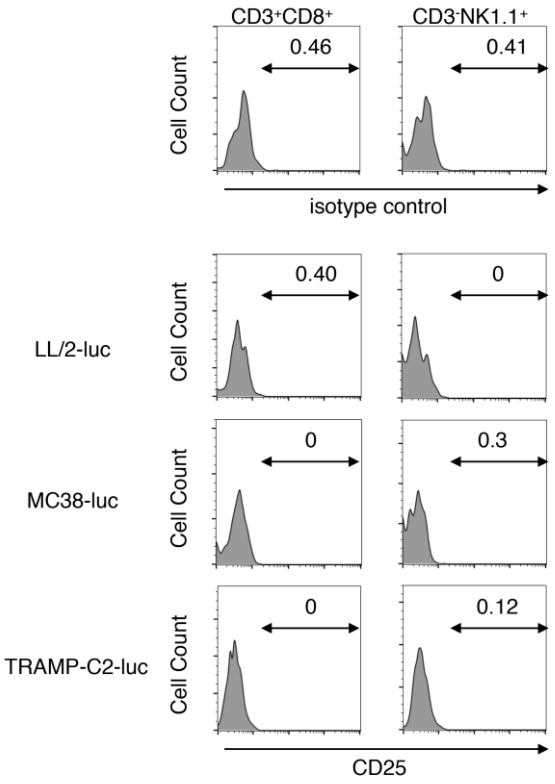

Supplementary Figure 3.

Tumor-infiltrating CD8 T and NK cells do not express CD25.

Flow cytometry analysis of CD8 T cells and NK cells collected from LL/2-luc, MC38-luc, or TRAMP-C2 tumors indicated that these cells did not express CD25.

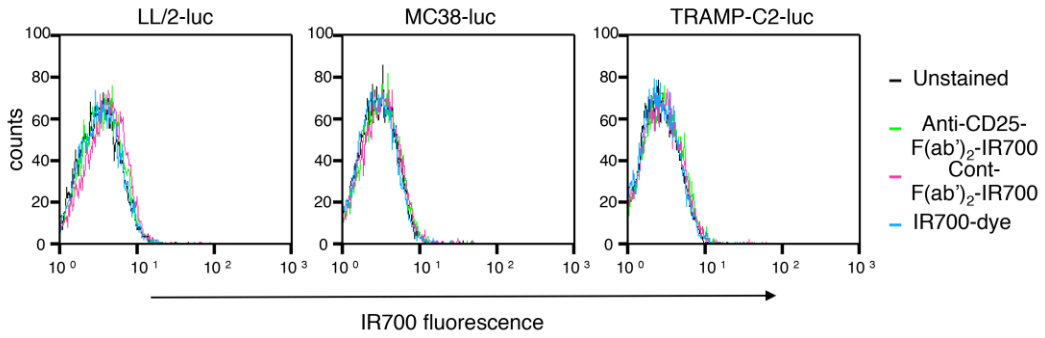

Supplementary Figure 4.

Anti-CD25-F(ab′)$_2$–IR700 does not bind to the tumor cells.

Anti-CD25-F(ab′)$_2$–IR700, cont-IgG-F(ab′)$_2$–IR700, or IR700 dye incubated with LL/2-luc, MC38-luc, or TRAMP-C2 tumor cells showed no binding by flow cytometry analysis.

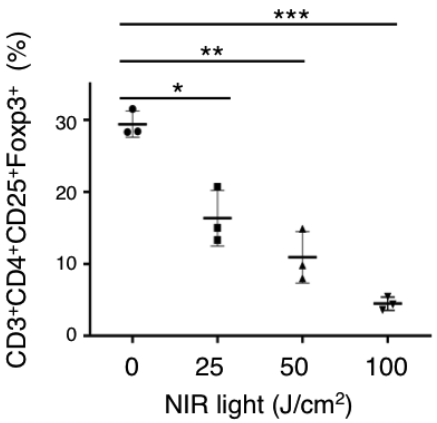

Supplementary Figure 5.

Depletion of tumor-infiltrating $CD4^+CD25^+Foxp3^+$ T_{regs} with local CD25-targeted NIR-PIT is NIR light dose–dependent.

Lymphocytes were collected from LL/2-luc tumors before and 30 min after local CD25-targeted NIR-PIT using increasing doses of NIR light. Flow cytometry analysis of the $CD4^+CD25^+Foxp3^+$ T_{reg} population within CD4 T cells indicated that T_{regs} decreased in a NIR light dose-dependent manner (n = 3; *p < 0.005, **p < 0.0005, ***p < 0.0001, vs. 0 J/cm^2, Tukey's test with ANOVA).

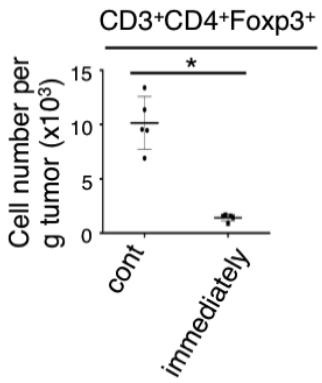

Supplementary Figure 6.

Tumor-infiltrating CD4$^+$Foxp3$^+$ cells are depleted by local CD25-targeted NIR-PIT.

Lymphocytes were collected from LL/2-luc tumors before and immediately (30 min) after local CD25-targeted NIR-PIT. Flow cytometry analysis of CD4$^+$Foxp3$^+$ cell number per gram indicated that CD4$^+$Foxp3$^+$ cells decreased after local CD25-targeted NIR-PIT (n = 5; *$p < 0.008$, Mann-Whitney test).

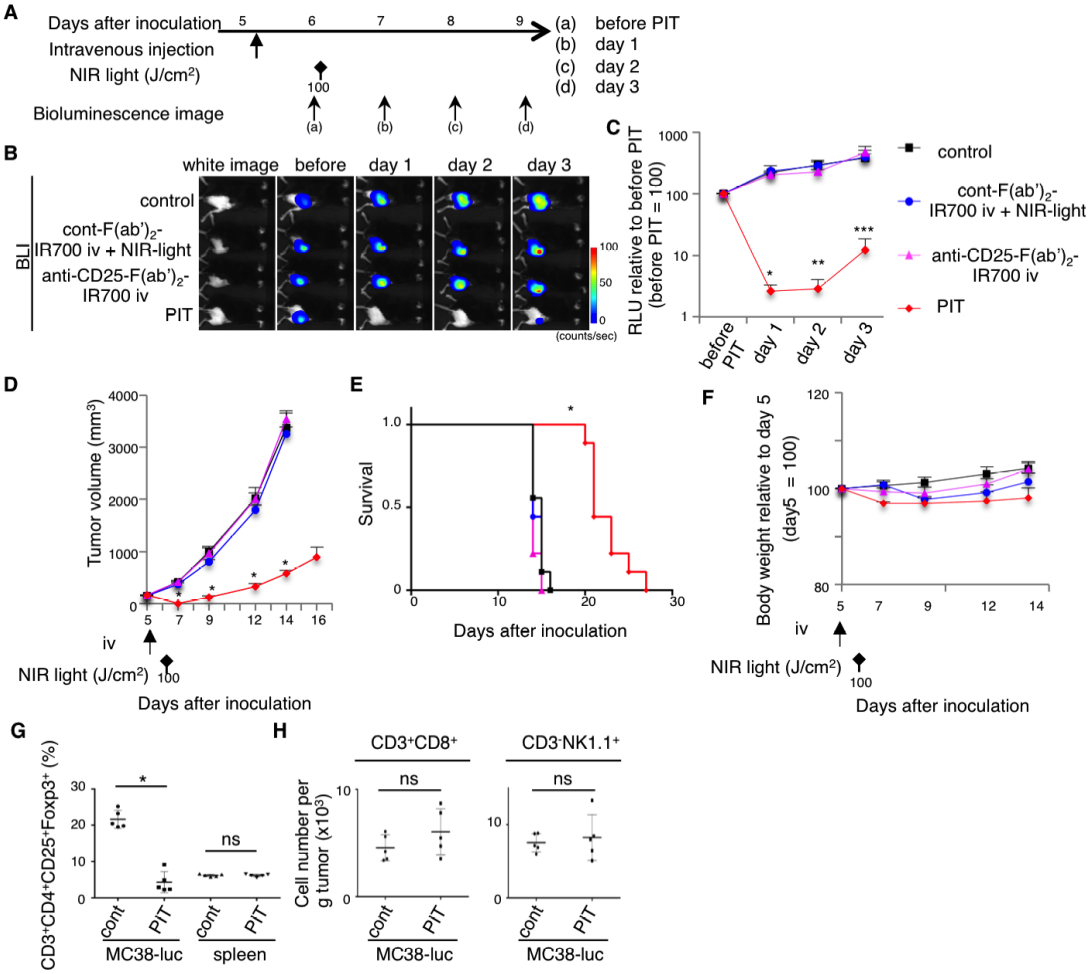

Supplementary Figure 7.

Local CD25-targeted NIR-PIT of an MC38-luc tumor induces regression of the tumor.

(A) The regimen of local NIR-PIT is shown. (B) In vivo BLI are shown for the tumor-bearing mice that were untreated, received a control-F(ab′)$_2$-IR700 followed by NIR-PIT, received CD25-F(ab′)$_2$-IR700 alone, or were treated with local CD25-targeted NIR-PIT. Only the CD25-targeted NIR-PIT resulted in a decrease of the signal. (C) Quantitative RLU showed a significant decrease in signal in the NIR-PIT-treated tumors (n

= 7 mice in each group; *p < 0.0005, **p < 0.005, ***p = 0.0268 (vs. control), 0.0236 (vs. control-F(ab′)$_2$-IR700 + NIR-light), 0.0056 (vs. anti-CD25-F(ab′)$_2$-IR700 iv), Tukey's test with ANOVA). (D) Local CD25-targeted NIR-PIT reduced tumor volume (n = 9 mice in each group; *p < 0.0001, PIT vs. others, Tukey's test with ANOVA) and (E) prolonged the survival of the mice (n = 9 mice in each group; *p < 0.0001, PIT vs. control, log-rank test and Wilcoxon test). (F) The groups of mice did not show significant differences in body weight during the course of the treatments (n = 9 mice in each group). (G) Local CD25-targeted NIR-PIT of the tumor resulted in the depletion of $CD4^+CD25^+Foxp3^+$ Tregs in the CD4 population (n = 5; *p < 0.01, ns: not significant, Mann-Whitney test) without affecting the Tregs in the spleen. (H) CD25-targeted NIR-PIT did not significantly affect the number of CD8 T cells ($CD3^+CD8^+$) or NK cells ($CD3^-NK1.1^+$) in the tumor (n = 5; (ns: not significant, Mann-Whitney test).

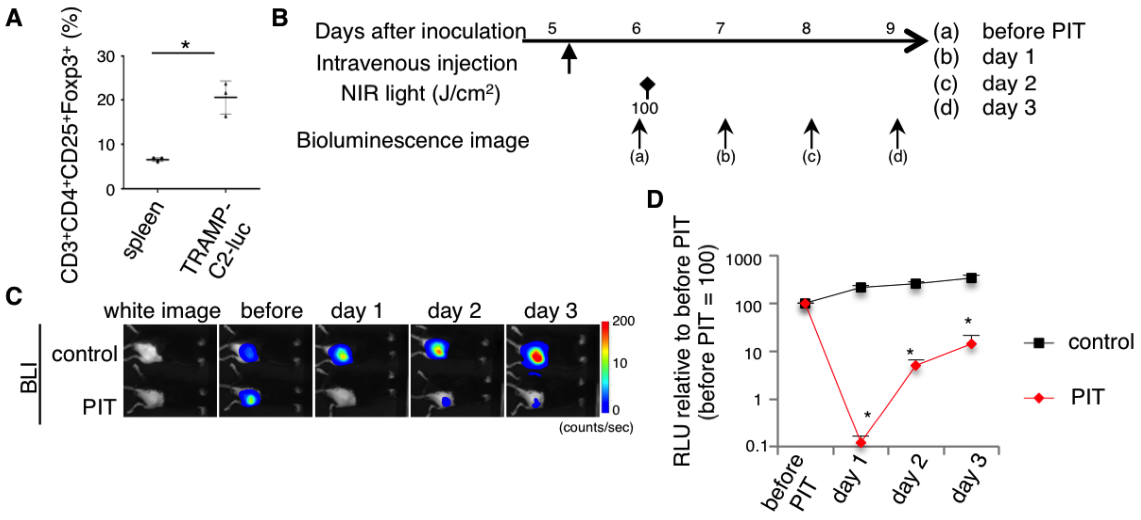

Supplementary Figure 8.

Local CD25-targeted NIR-PIT induces regression of TRAMP-C2-luc flank tumors.

(A) The fraction of $CD4^+CD25^+Foxp3^+$ Tregs within CD4 T cells was increased in TRAMP-C2-luc tumors compared to the spleen (n = 3; *p = 0.003, Mann-Whitney test). (B) The regimen of local NIR-PIT is shown. (C) In vivo BLI of tumor-bearing mice indicated a decrease of the bioluminescent signal in the tumor by CD25-targeted NIR-PIT. (D) Quantitative RLU showed a significant decrease of the signal in NIR-PIT-treated tumors (n = 5 mice in each group; *p < 0.008, PIT vs. control, Mann-Whitney test).

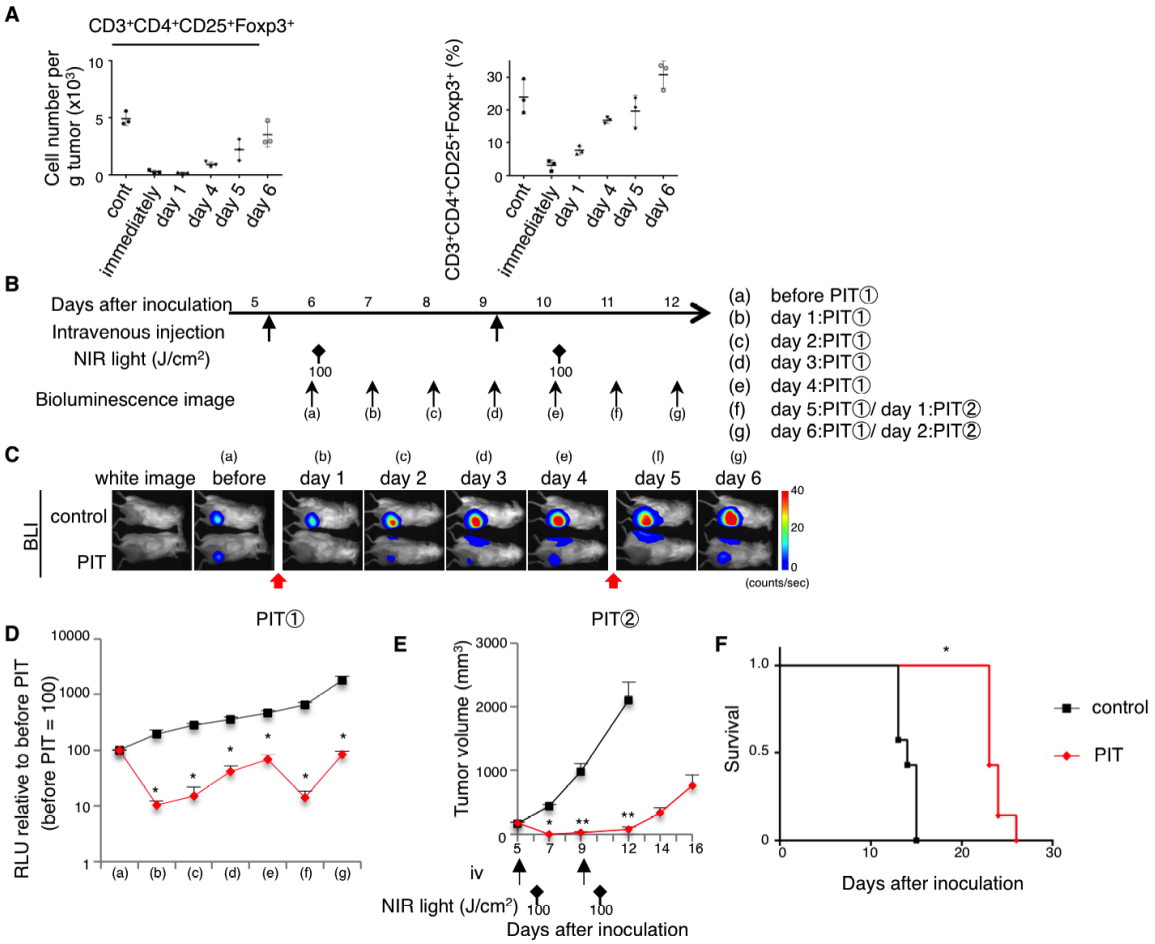

Supplementary Figure 9.

Repeated local CD25-targeted NIR-PIT enables prolonged suppression of tumor growth.

(A) Flow cytometry analysis of lymphocytes collected from LL/2-luc tumors after local CD25-targeted NIR-PIT indicated that the depletion of intratumoral $CD4^+CD25^+Foxp3^+$ Tregs lasted for about 4 days, after which they gradually re-populated in the tumor bed (n = 3). (B) The regimen of repeated local NIR-PIT is shown. The first PIT is indicated as PIT①, the second, repeated PIT as PIT②. (C) BLI indicated that a repeated local CD25-targeted

NIR-PIT of LL/2-luc tumor inoculated in albino mice was capable of inducing tumor regression repeatedly. (D) Quantitative RLU shows a significant decrease in signal in the NIR-PIT-treated tumors (n = 7 mice in each group; *p < 0.001, Mann-Whitney test). (E) Repeated local CD25-targeted NIR-PIT reduced tumor volume (n = 7 mice in each group; *p < 0.01, **p < 0.001, Mann-Whitney test) and (F) prolonged the survival of the mice (*p < 0.0001, log-rank test and Wilcoxon test).

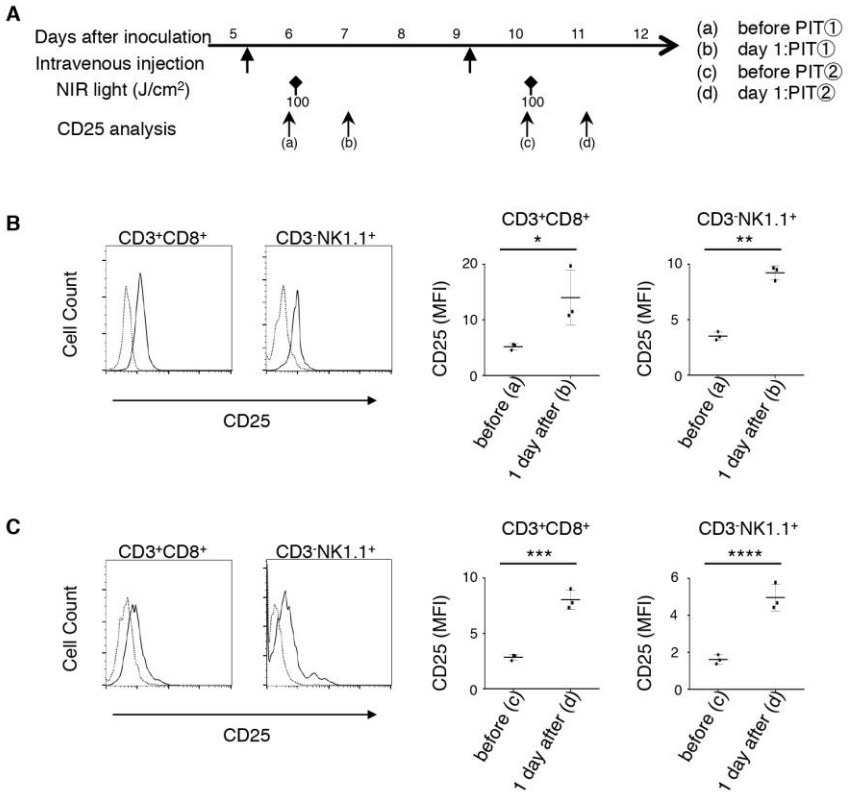

Supplementary Figure 10.

Repeated local CD25-targeted NIR-PIT induces up-regulation of CD25 on CD8 T and NK cells at each treatment.

(A) The regimen of analysis of CD25 expression in repeated local NIR-PIT is shown. (B) MFI (geometric mean fluorescence intensity) of CD25 expression was increased after the first local CD25-targeted NIR-PIT (n = 3; *p = 0.0376, **p < 0.0005, unpaired t test). The broken and solid lines indicate CD25 expression before and 1 day after the NIR-PIT, respectively. (C) Four days after the first NIR-PIT, the expression of CD25 (solid line) returned to the pre-treatment baseline (broken line). The second local NIR-PIT induced activation and up-regulation of CD25 expression on CD8 T and NK cells again (n = 3; ***p < 0.001, ****p < 0.005, unpaired t test).

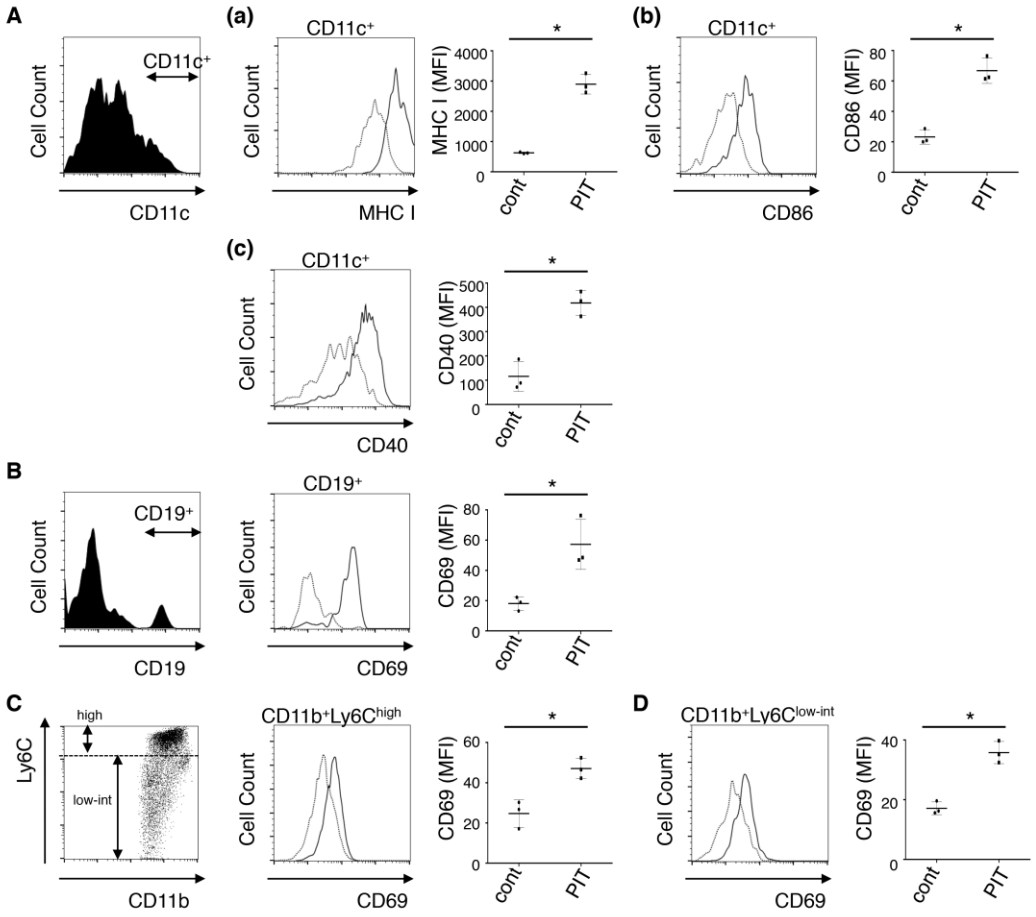

Supplementary Figure 11.

Local CD25-targeted NIR-PIT induces activation of tumor-infiltrating dendritic cells and other APCs.

Flow cytometry of tumor-infiltrating immune cells indicated that CD25-targeted NIR-PIT induced activation of tumor-infiltrating (A) dendritic cells ($CD11c^+$), (B) B cells ($CD19^+$), (C) monocytes ($CD11b^+Ly6C^{high}$), and (D) macrophages ($CD11b^+Ly6C^{low\text{-}int}$) 1 day after the treatment (n = 3; *p = 0.0104, unpaired t test; solid line: specific antibody, broken line: isotype control antibody). The population of the analysis is indicated in the left side panel.

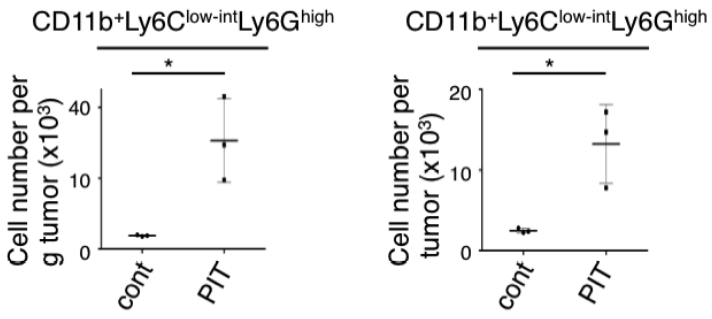

Supplementary Figure 12.

Local CD25-targeted NIR-PIT increases the number of granulocytes in treated tumors.

Flow cytometry analysis of tumor-infiltrating granulocytes ($CD11b^{+}Ly6C^{low\text{-}int}Ly6G^{high}$) indicated that local CD25-targeted NIR-PIT induced an increase in these cells [n = 3; *p = 0.0188 (per g tumor), 0.0168 (per tumor), unpaired t test]. Cell number per g tumor and per tumor are both shown.

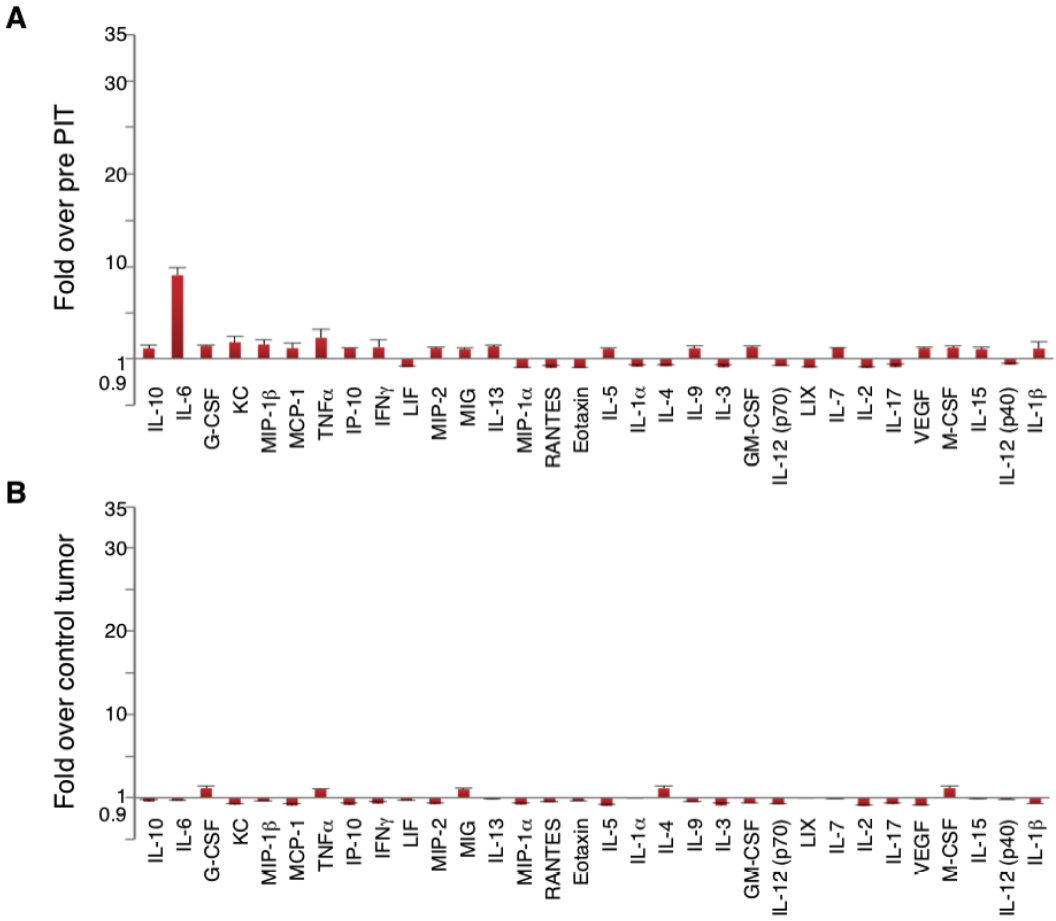

Supplementary Figure 13.

NIR light irradiation of tumors induces negligible production of cytokines and chemokines.

(A) Serum cytokine and chemokine concentrations before and 1.5 hours after NIR light irradiation at the tumor were sequentially measured in each mouse. The results are indicated as fold increase (n =3). (B) Cytokine and chemokine concentrations within the tumor were compared between mice with NIR light irradiated tumors and mice with untreated tumors. Tumors were harvested for collecting extracellular fluid at 1.5 hours (n =3).

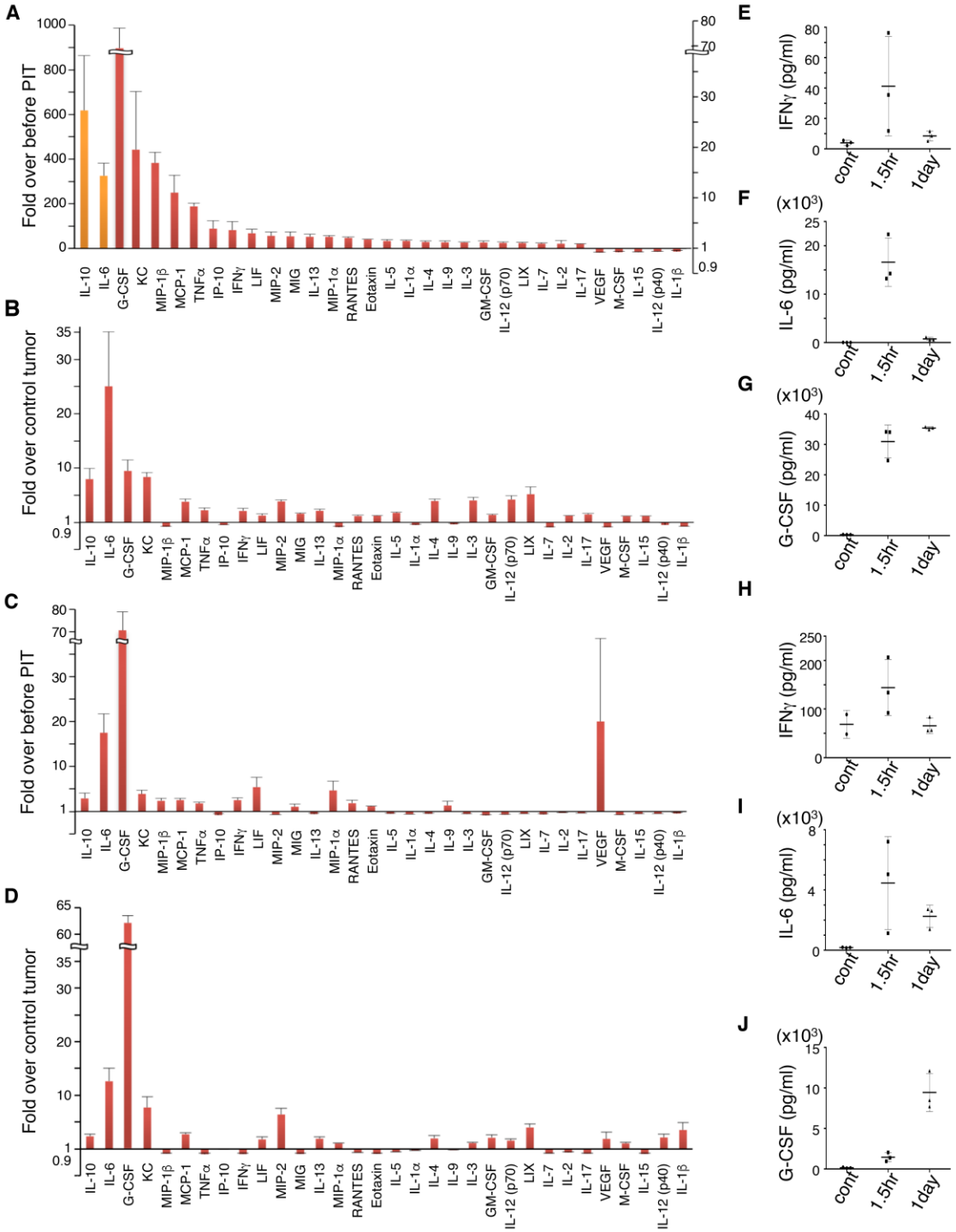
A
Fold over before PIT
B
Fold over control tumor
C
Fold over before PIT
D
Fold over control tumor
IL-10
IL-6
G-CSF
KC
MIP-1β
MCP-1
TNFα
IP-10
IFNγ
LIF
MIP-2
MIG
IL-13
MIP-1α
RANTES
Eotaxin
IL-5
IL-1α
IL-4
IL-9
IL-3
GM-CSF
IL-12 (p70)
LIX
IL-7
IL-2
IL-17
VEGF
M-CSF
IL-15
IL-12 (p40)
IL-1β
E
IFNγ (pg/ml)
F
(x10³)
IL-6 (pg/ml)
G
(x10³)
G-CSF (pg/ml)
H
IFNγ (pg/ml)
I
(x10³)
IL-6 (pg/ml)
J
(x10³)
G-CSF (pg/ml)
cont
1.5hr
1day

Supplementary Figure 14.

Local CD25-targeted NIR-PIT induces systemic and intratumoral cytokine storm.

(A) Serum cytokine and chemokine concentrations before and 1.5 hours after local CD25-targeted NIR-PIT of tumors were sequentially measured before and after treatment in each mouse. The results are indicated as fold increase (IL-10 and IL-6 on the left axis and others on the right axis) (n =3). (B) Similarly, intratumoral cytokine and chemokine concentrations were compared before and 1 day after NIR-PIT (n =3). Cytokine and chemokine concentrations within the tumor were compared between mice with treated tumors and mice with untreated tumors. Tumors were harvested for collecting extra cellular fluid at 1.5 hours (C) and 1 day (D) after NIR-PIT (n =3). (E-G) Serum concentrations of (E) IFNγ, (F) IL-6, and (G) G-CSF (n =3). (H-J) Intratumoral concentrations of (H) IFNγ, (I) IL-6, and (J) G-CSF (n =3).

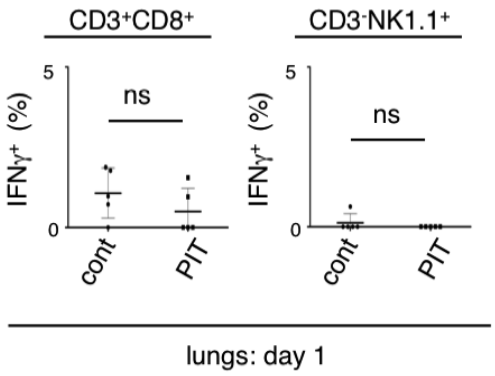

Supplementary Figure 15.

IFN-γ production by CD8 T and NK cells in the lungs is not detected 1 day after CD25-targeted NIR-PIT.

IFNγ production was not detected by flow cytometry assay in the CD8 T cells and NK cells collected from the lungs 1 day after CD25-targeted NIR-PIT. (n = 5; ns: not significant, Mann-Whitney test).

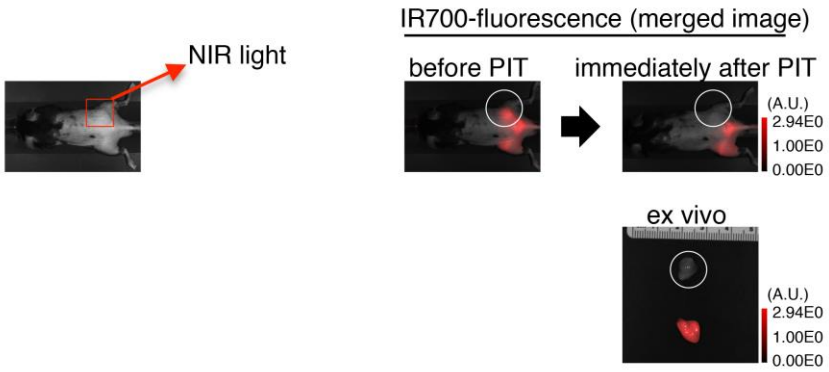

Supplementary Figure 16.

CD25-targeted NIR-PIT reduces IR700 fluorescence of the treated tumor, but not that of the contralateral nonirradiated tumor.

IR700 fluorescence decreased after local CD25-targeted NIR-PIT within the right-sided LL/2-luc tumor, but no change in fluorescence was seen in the left, nonirradiated tumor. IR700-fluorescence imaging of ex vivo tumors is also demonstrated.

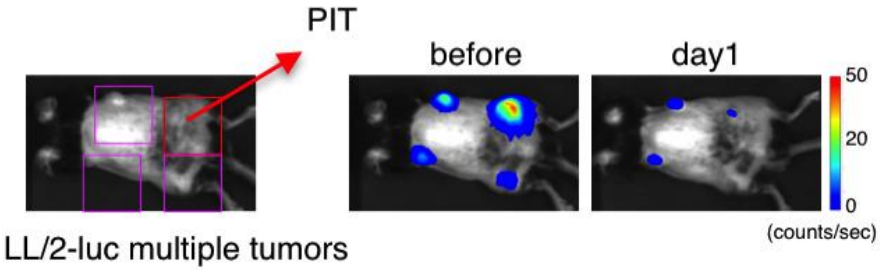

Supplementary Figure 17.

Local CD25-targeted NIR-PIT of the right dorsal tumor induces reduction of multiple tumors at distant sites.

Local CD25-targeted NIR-PIT of the right dorsal LL/2-luc tumor caused regression of multiple other LL/2-luc tumors located at distant sites at 1 day after the treatment (different mouse from the experiment shown in Fig. 4J).

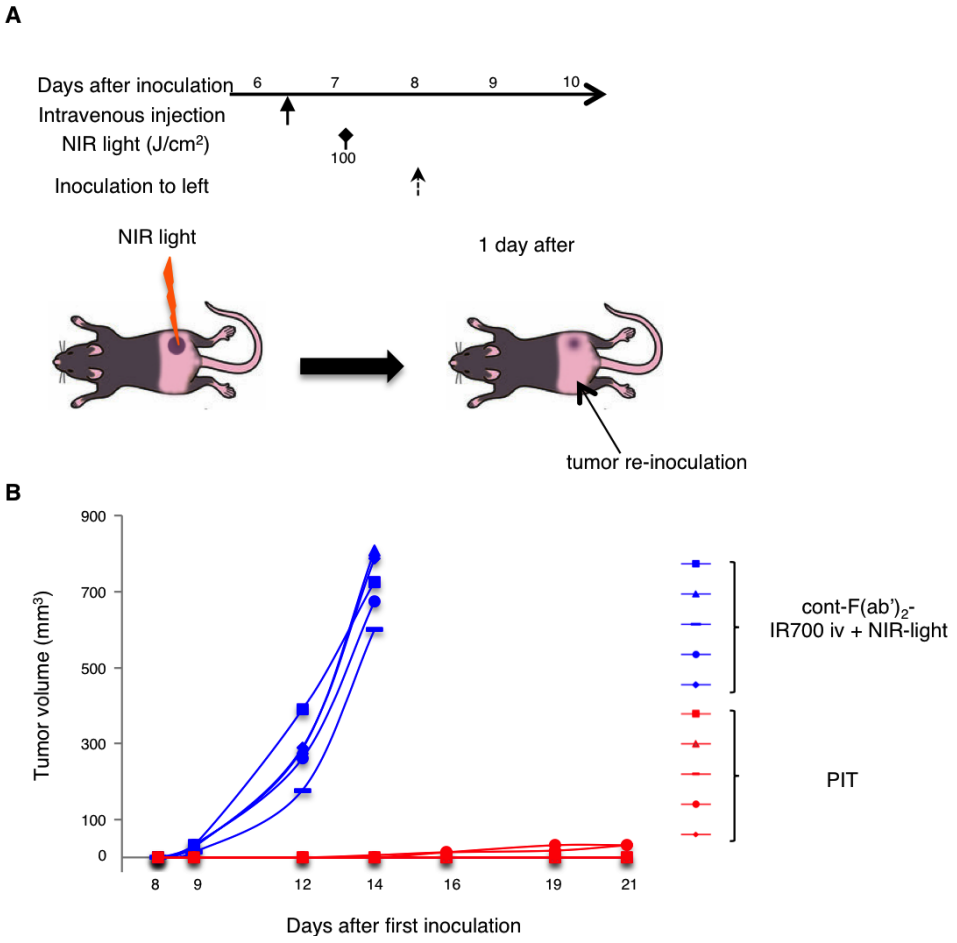

Supplementary Figure 18.

Local CD25-targeted NIR-PIT inhibits the growth of tumor challenged on the contralateral side.

(A) The regimen of tumor challenge at 1 day after CD25-targeted NIR-PIT is shown. A schematic representation is also provided. (B) The growth of LL/2-luc tumor inoculated on the contralateral side 1 day after local CD25-targeted NIR-PIT of the same tumor type was inhibited compared to the tumor inoculated into control mice receiving control-F(ab′)$_2$-IR700 administration with NIR light irradiation (n =5 per group).

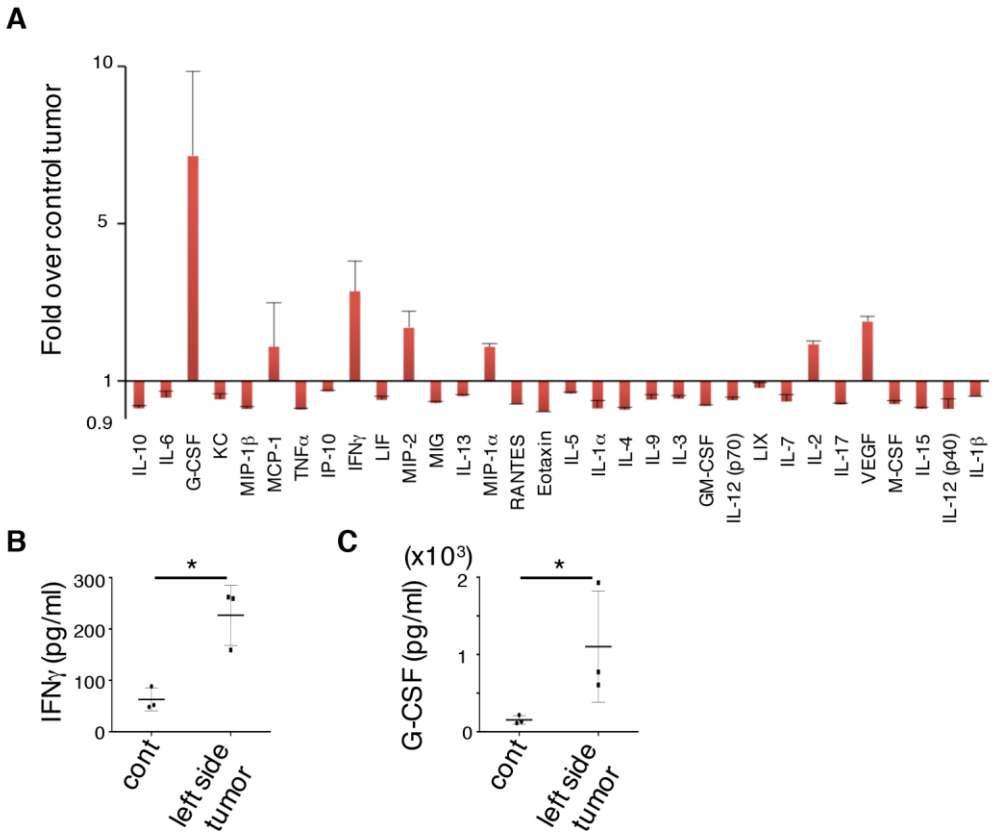

Supplementary Figure 19.

The concentrations of cytokines and chemokines in the contralateral nonirradiated tumor are increased after CD25-targeted NIR-PIT.

(A) Non-irradiated left dorsal tumor had increased cytokine/chemokine concentrations in response to CD25-targeted NIR-PIT of the contralateral tumor at 1 day after the therapy (n = 3). (B-C) In the left side nonirradiated tumor, concentrations of (B) IFNγ and (C) G-CSF were increased (n = 3; *p = 0.0107 (B), *p = 0.0353 (C), unpaired t test).

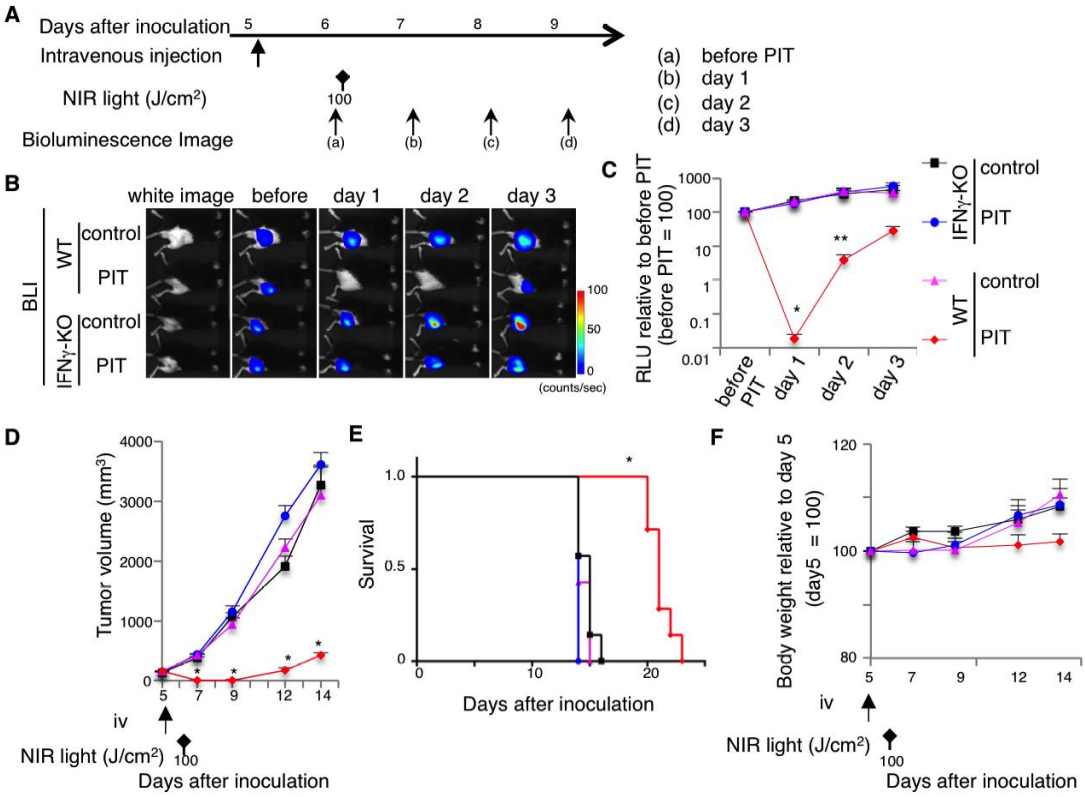

Supplementary Figure 20.

Antitumor effect of local CD25-targeted NIR-PIT is at least partly IFN-γ–dependent.

(A) The regimen of NIR-PIT is shown. (B) In vivo BLI of LL/2-luc tumors in response to local CD25-targeted NIR-PIT in wild type (WT) and IFN-γ–deficient (IFNγ-KO) mice indicated that only the NIR-PIT-treated tumor in the WT mice demonstrated a decrease in bioluminescence signal at days 1-3. (C) Quantitative RLU shows a significant decrease in NIR-PIT-treated tumors in WT mice, but not in those in IFNγ-KO mice (n = 5 mice in each group; *$p < 0.0005$, **$p = 0.0422$ (vs. WT-control), 0.0315 (vs. KO-control), 0.0255 (vs. KO-PIT), WT-PIT vs. others, Tukey's test with ANOVA). (D) Local CD25-targeted NIR-PIT reduced the tumor volume of NIR-PIT-treated tumors in WT mice, whereas the

anti-tumor effects of local NIR-PIT in IFNγ-KO mice were not significant (n=7 mice in each group; *p < 0.0001, WT-PIT vs. others, Tukey's test with ANOVA, treatments are indicated below the graph). (E) Survival curves of PIT-treated WT and IFNγ-KO mice bearing LL/2-luc tumors indicated that the deficiency of IFN-γ at least partly abrogated the treatment effects (n = 7 mice in each group; *p < 0.0001 vs. WT-control, log-rank test and Wilcoxon test). (F) WT and IFNγ-KO mice did not show significant differences in body weight (n = 7 mice in each group, Tukey's test with ANOVA).